STATE ESTIMATION AND EXPERIMENTAL VERIFICATION OF A ROBOTIC VEHICLE WITH SIX IN-WHEEL DRIVES USING KALMAN FILTER

Hussein F. M. Ali[1,2]
[1]Mechanical Engineering, Benha University, Benha, Egypt

Se-Woong Oh[2], **Youngshik Kim**[2]
[2]Mechanical Engineering, Hanbat National University Daejeon, Korea

ABSTRACT

In this research we present an algorithm for a six-wheeled robotic vehicle with articulated suspension (RVAS) to estimate the vehicle velocity and acceleration states, slip ratio and the tire forces. The estimation algorithm consists of six parts. In the first part, a wheel state estimator estimates the wheel rotational speed and its angular acceleration using Kalman filter, which is used to estimate the longitudinal tire force distribution in the second part. The third part is to estimate respective longitudinal, lateral, and vertical speeds of the vehicle and wheels. Based on these speeds, the slip ratio and slip angle are estimated in the fourth part. In the fifth part, the vertical tire force is then estimated. In the sixth part, the lateral tire force is then estimated. For a simulation test environment, the RVAS dynamic model is developed using Matlab and Simulink. The estimation algorithm is then verified in simulation using the vehicle test data and different test scenarios. It is found from simulation results that the proposed estimation algorithm can estimate the vehicle states, longitudinal tire forces efficiently. Moreover, a small prototype of the robotic vehicle is fabricated for experimental verification of the estimation algorithm. Various experiments are executed in pavement and off-road driving to estimate the wheel angular position, velocity and acceleration states and finally the slip ratio is estimated in these situations.

Keywords: state estimation, Kalman filter, robotic vehicle with articulated suspension, slip ratio estimation, Fiala tire model, tire forces.

NOMENCLATURE

g gravity acceleration
c_d rotational damping coefficient of the arm rod
I_x, I_y, I_z moments of inertia of the vehicle about the roll, pitch and yaw axes respectively
$I_{arm\_x}, I_{arm_y}, I_{arm\_z}$ moments of inertia of the arm rod about the roll, pitch and yaw axes respectively
I_{w_x} moment of inertia of the wheel about the roll axis
I_{w_z} moment of inertia of the wheel about the yaw axis
J_w moment of inertia of the wheel about its rotational axis
k_s rotational spring stiffness of the arm rod
l_{arm} length of the arm rod
l_f distance from the vehicle c.g to the front arm axle
l_m distance from the vehicle c.g. to the middle arm axle
l_r distance from the vehicle c.g. to the rear arm axle
m_{arm}, m_s, m_w masses of the arm rod, sprung mass of the vehicle and the in-wheel motor respectively
M_{sxi} internal moment acting on the sprung mass about the roll axis at the rotational center of the i^{th} arm rod
M_{szi} internal moment acting on the sprung mass about the yaw axis at the rotational center of the i^{th} arm rod

E-mail: hussein.ali@ejust.edu.eg; osw9209@naver.com;
[2] Corresponding author: youngshik@hanbat.ac.kr

M_{z_des} yaw moment input
t_w half of the vehicle width
ω_{arm_i} angular velocity vector of the i^{th} arm rod
ω_{cg} vehicle angular velocity vector
ω_i angular speed at the i^{th} wheel
$\hat{\omega}_i$ estimated angular speed at the i^{th} wheel
$\theta_{arm_i}(0)$ initial arm angle at time 0
R tire radius of the i^{th} wheel
λ_i slip ratio at the i^{th} wheel
$F_{sxi}, F_{syi}, F_{szi}$ longitudinal, lateral, and vertical internal forces acting on a sprung mass at the rotational center of the i^{th} arm rod respectively
$F_{txi}, F_{tyi}, F_{tzi}$: longitudinal, lateral, and vertical tire forces at the i^{th} wheel respectively
$\dot{r}_{cg}$, $\ddot{r}_{cg}$ vehicle velocity, and acceleration vectors
$\ddot{r}_i$ translational acceleration vector of the rotational center of the i^{th} arm rod
$\ddot{r}_{wi}$ translational acceleration vector of the i^{th} wheel
T_i measured wheel torque of the i^{th} wheel
T_{self_i} self-aligning torque at the i^{th} wheel
$T_{S\&D\_i}$ sum of spring and damping torques of the i^{th} arm rod
v_x, v_y, v_z Vehicle longitudinal, lateral & vertical velocities
α_i slip angle at the i^{th} wheel
α_{cg} vehicle angular acceleration vector
α_{arm_i} angular acceleration vector of the i^{th} arm rod
$\dot{\phi}, \dot{\theta}, \dot{\varphi}$ roll rate, pitch rate, yaw rate
$\theta_{arm\_i}, \theta_{arm\_static}$ arm angle at i^{th} arm rod, and static arm

1. INTRODUCTION

States estimation of autonomous vehicle has received appreciable attention in the recent decades. States estimation is necessary in vehicle stability and motion control, specially when it is difficult to measure some states or the sensor data is noisy. In earlier stages, most research was based on the kinematic model of a wheeled mobile robot where the input was velocity. The dynamic modeling and forces estimation have a significant impact on the control and the stability of those autonomous vehicle specially when it is difficult to measure some states or forces [1].

In order to describe the vehicle movements, we need numerous measurements and kinematic and dynamic modeling, which represent the system behavior. The fineness degree of modeling depends on the main objectives. For a simulator design, modeling efforts focus on reproducing the vehicle components behavior as precisely as possible. Simulations of full vehicle kinematics and dynamics models are typically computationally expensive and time-consuming. However, for high performance vehicle controllers, simplifications are needed to do only the necessary computation in real-time [2]. Tire forces influence largely the chassis stability and maneuverability [3]. These forces are limited by the maximum friction that can be generated between the tire carcass and the road surface, which is the result of complex phenomena on the rubber-road interface. A

comprehensive list of relevant real-time tire force estimation methods can be found in [4]and offline approaches [5,6,7].

Many Kalman filters are used for state estimation. E. Nada et al., [8] presented a modified dual unscented Kalman filter (MDUKF) approach to estimate vehicle states and vehicle parameters to improving performance of AVs due to the nonlinear characteristic of tire-road. K. Yi et al., [9] described torque distribution control algorithm of six-wheeled vehicles using the friction circle of each wheel. H. Hamann et al., [10] used Unscented Kalman filter (UKF) for tire force estimation for a vehicle with standard sensors and no knowledge of tire and road properties. A. Rezaeian et al., [11] proposed an algorithm to estimate tire forces by nonlinear observers. The estimations are robust against changes in vehicle/ road parameters like mass and even wear and road conditions. The lateral tire forces were estimated by using the estimated vertical and longitudinal tire forces from the previous two modules and Extended Kalman filter (EKF) and UKF. A. Zareian et al., [12] developed an estimation algorithm for road friction coefficient using extended Kalman filter, recursive least square, and neural network.

Recently in [13, 14] we presented a comparative study of EKF and UKF for estimating motion states of an autonomous vehicle-trailer system. The system is equipped with the GPS, odometry, and hitch angle sensors. The simulations indicate that both EKF and UKF give the same accurate result but the processing time is increase by 17.7% for UKF.

For robotic vehicles with six in-wheel drives, K. Yi et al., [15] presented skid steering-based control which utilizes the tire states estimation. However, the lateral forces estimation was not addressed.

In a previous work, we presented the state estimation algorithm of the robotic vehicle with six in-wheel drives. WE started with the estimation of wheel angular acceleration using Kalman filter then the longitudinal tires forces, vertical tires forces, and lateral tires forces are estimated [16]. In this work, we fabricated a small-scale prototype of the robotic vehicle for experimental verification of the previous simulation results specially the angular acceleration estimation and the slip ratio estimation. Then we presented a detailed procedure to calculate the nonlinear motor torque constant and to estimate the longitudinal tire forces experimentally.

In this paper, section 2 presents the dynamic model of a 6-wheel vehicle including the driving system, the arm dynamic model, and the sprung mass dynamic model. Section 3 presents the estimation algorithm based on Kalman filter and manipulated dynamic equation. Then the simulation is presented in section 4. Finally, in section 5, we presented the experimental results and discussion.

2. SYSTEM DYNAMIC MODELING

In this section, the dynamic model of a six-wheel vehicle with articulated suspension (RVAS) shown in Fig.1 is presented for the vehicle forces estimation algorithm. The RVAS is an unmanned ground vehicle based on a skid steering using an independent in-wheel motor at each wheel. The RVAS model is implemented in section 3 using Simulink/Matlab as a test environment. The dynamic model consists of five main parts: in-wheel motor model, wheel dynamic model, Fiala tire model, arm dynamic model, and the sprung mass dynamic model.

The dynamic model is 18 DOF with the dynamic equations of six wheels, six connective arm rods, and a sprung mass. The sprung mass is modeled as rigid body connected to the arm rods. The sprung mass has 6 DOF translational motions (longitudinal, lateral, and vertical) and rotational motions (roll, pitch, and yaw). The RVAS 6-wheel vehicle dynamic model includes three parts: driving system, arm dynamic model, and sprung mass dynamic model, shown in Fig.2.

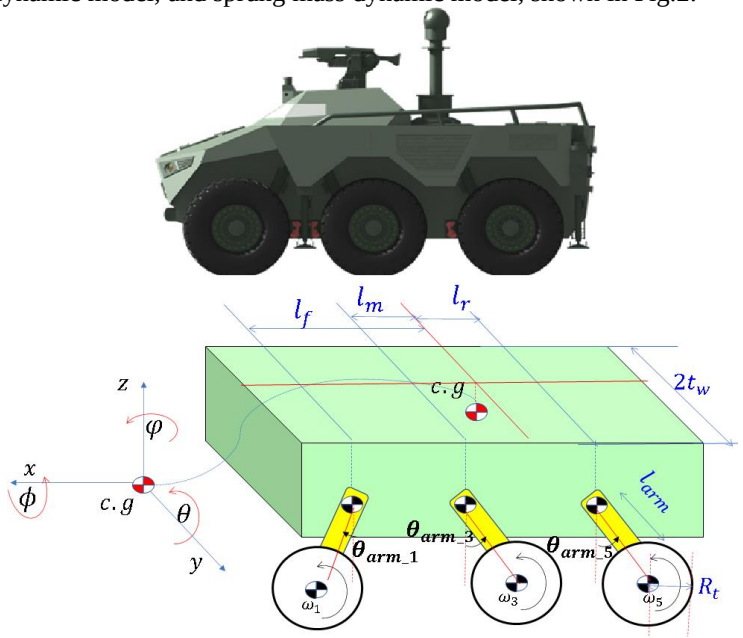

Fig. 1: 6-wheel Vehicle Model

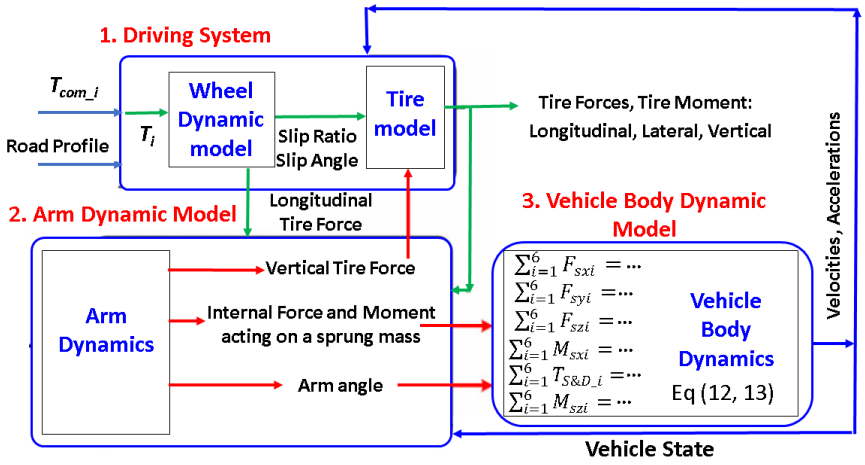

Fig. 2: Schematic Diagram of the Dynamic Model

2.1 Driving system

The driving system contains an in-wheel motor model, a wheel dynamic model, and a tire model. By applying the simplified wheel free-body diagram in Fig.3, the wheel dynamic model is determined by,

$$J_w \times \frac{d\omega_i(t)}{dt} = \mathrm{T_i}(t) - R_i F_{txi(t)} \quad \ldots\ldots\ldots\ldots\ldots\ldots\ldots\ldots\ldots\ldots\ldots\ldots (1)$$

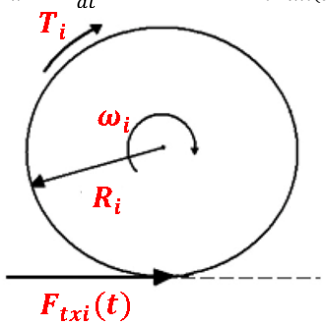

Fig. 3: Free body diagram of the wheel

Fiala tire model is then used to calculate the tire forces and moments [17] as shown in Fig.4. where (C_α=13.963 N/rad, CSLIP=1kN/m). According to the magic formula tire model [15], the slip ratio and the slip angle are expressed by,

$$\lambda_\mathrm{i} = \begin{cases} \frac{R_i \times w_i - v_{txi}}{R_i \times w_i} & if(\lambda_\mathrm{i} > 0) \\ \frac{R_i \times w_i - v_{txi}}{v_{txi}} & if(\lambda_\mathrm{i} \leq 0) \end{cases}, \alpha_\mathrm{i} = -\tan^{-1}\left(\frac{v_{tyi}}{v_{txi}}\right) \quad \ldots\ldots\ldots\ldots\ldots\ldots (2)$$

Tire center velocity vector (longitudinal, lateral, vertical) can be calculated considering the relative rigid body motion by,

$$\dot{r}_{\mathrm{wi}} = \begin{bmatrix} v_{\mathrm{txi}} & v_{\mathrm{tyi}} & v_{\mathrm{tzi}} \end{bmatrix}^{\mathrm{T}} = \dot{r}_{\mathrm{cg}} + \omega_{\mathrm{cg}} \times \mathrm{r}_{\mathrm{i/cg}} + \omega_{\mathrm{arm\_i/cg}} \times \mathrm{r}_{\mathrm{wi/i}}$$
$$= \begin{bmatrix} v_x \\ v_y \\ v_z \end{bmatrix} + \begin{bmatrix} \dot{\phi} \\ \dot{\theta} \\ \dot{\varphi} \end{bmatrix} \times \begin{bmatrix} l_i \\ \pm t_w \\ 0 \end{bmatrix} + \begin{bmatrix} 0 \\ \dot{\theta}_{arm\_i} \\ 0 \end{bmatrix} \times \begin{bmatrix} -l_{arm} \sin(\theta_{arm\_i}) \\ 0 \\ -l_{arm} \cos(\theta_{arm\_i}) \end{bmatrix} \quad \ldots\ldots\ldots\ldots\ldots (3)$$

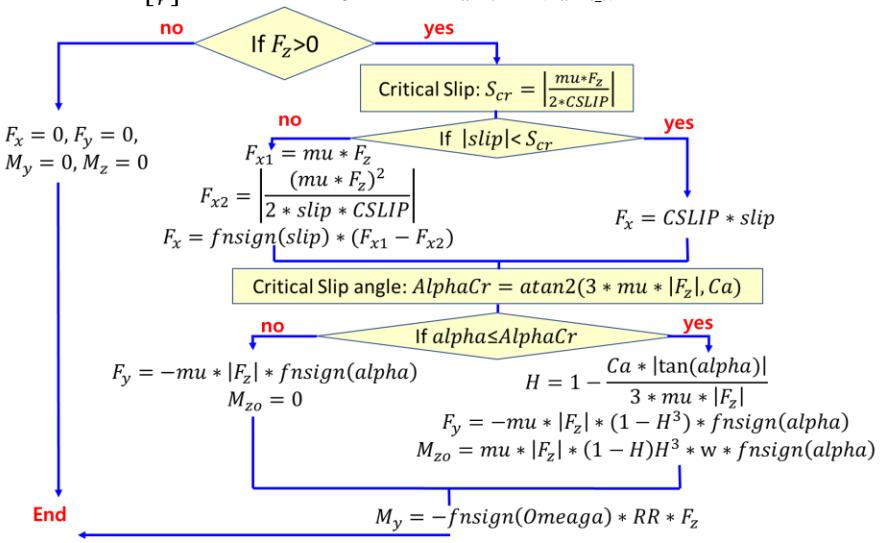

Fig. 4: Schematic diagram of Fiala tire model implementation

2.2 Arm dynamic model

The arm dynamic model is determined using the equations of motions 4, and 5: which can be derived considering dynamic equilibrium of the arm and the wheel, as shown in Fig.5,

$\sum F_{x\_arm\_i} = F_{txi} - F_{sxi} = (m_{arm} \times \ddot{x}_{arm,i}) + (m_w \times \ddot{x}_{w\_i})$
$\sum F_{y\_arm\_i} = F_{tyi} - F_{syi} = (m_{arm} \times \ddot{y}_{arm,i}) + (m_w \times \ddot{y}_{w\_i})$
$\sum F_{z\_arm\_i} = F_{tzi} - F_{szi} - (m_w + m_{arm}) \cdot g = (m_{arm} \times \ddot{z}_{arm\_i}) + (m_w \times \ddot{z}_{w\_i})$ ….(4)
$\sum M_{x\_arm\_i} = I_{arm\_x} \times \alpha_{arm\_xi} + (I_{arm\_z} - I_{arm\_y}) \times \omega_{arm\_yi} \times \omega_{arm\_zi} + l_{arm} \times \cos(\theta_{arm\_i})\,(m_w \times \ddot{y}_{wi} + m_{arm}\frac{\ddot{y}_{arm\_i}}{2})$
$\sum M_{y\_arm\_i} = I_{arm\_y} \times \alpha_{arm\_yi} + (I_{arm\_x} - I_{arm\_z}) \times \omega_{arm\_zi} \times \omega_{arm\_xi} - \left(m_w \times \ddot{x}_{wi} + m_{arm}\frac{\ddot{x}_{arm\_i}}{2}\right) l_{arm} \times \cos(\theta_{arm\_i}) + (m_w \times \ddot{z}_{wi} + m_{arm}\frac{\ddot{z}_{arm\_i}}{2}) l_{arm} \times \sin(\theta_{arm\_i})$
$\sum M_{z\_arm\_i} = I_{arm\_z} \times \alpha_{arm\_zi} + (I_{arm\_y} - I_{arm\_x}) \times \omega_{arm\_xi} \times \omega_{arm\_yi} - l_{arm} \times \sin(\theta_{arm\_i})\,(m_w \times \ddot{y}_{wi} + m_{arm}\frac{\ddot{y}_{arm\_i}}{2})$ ………………………………………. (5)

The angular velocity vector of the i^{th} arm rod can be expressed in relative to the vehicle orientation rates by,

$$\omega_{\text{arm\_i}} = [\omega_{\text{arm\_xi}} \quad \omega_{\text{arm\_yi}} \quad \omega_{\text{arm\_zi}}]^{\text{T}} = \omega_{\text{cg}} + \omega_{\text{arm\_i/cg}} = [\dot{\phi} \quad \dot{\theta} + \dot{\theta}_{arm\_i} \quad \dot{\varphi}]^T \quad (6)$$

Similarly, the angular acceleration vector of the i^{th} arm rod can be written with respect to the vehicle center by,

$$\alpha_{\text{arm\_i}} = [\alpha_{\text{arm\_xi}} \quad \alpha_{\text{arm\_yi}} \quad \alpha_{\text{arm\_zi}}]^{\text{T}} = \alpha_{\text{cg}} + \alpha_{\text{arm\_i/cg}} + \omega_{\text{cg}} \times \omega_{\text{arm\_i/cg}}$$

$$= \begin{bmatrix}\ddot{\phi}\\ \ddot{\theta}\\ \ddot{\varphi}\end{bmatrix} + \begin{bmatrix}0\\ \ddot{\theta}_{arm\_i}\\ 0\end{bmatrix} + \begin{bmatrix}\dot{\phi}\\ \dot{\theta}\\ \dot{\varphi}\end{bmatrix} \times \begin{bmatrix}0\\ \dot{\theta}_{arm\_i}\\ 0\end{bmatrix} = \begin{bmatrix}\ddot{\phi} - \dot{\theta}_{arm\_i} \times \dot{\varphi}\\ \ddot{\theta} + \ddot{\theta}_{arm\_i}\\ \ddot{\varphi} + \dot{\theta}_{arm\_i} \times \dot{\phi}\end{bmatrix} \quad (7)$$

The translational acceleration vector of the i^{th} wheel can be obtained by,

$$\ddot{r}_{\text{wi}} = [\ddot{x}_{\text{wi}}\ \ddot{y}_{\text{wi}}\ \ddot{z}_{\text{wi}}]^{\text{T}} = \ddot{r}_{\text{i}} + \omega_{\text{arm\_i}} \times [\omega_{\text{arm\_i}} \times r_{wi/i}] + \alpha_{\text{arm\_i}} \times r_{wi/i}$$

The translational acceleration vector of the rotational center of the i^{th} arm rod is,

$$\ddot{r}_{\text{i}} = [\ddot{x}_{\text{i}}\ \ddot{y}_{\text{i}}\ \ddot{z}_{\text{i}}]^{\text{T}} = \ddot{r}_{\text{cg}} + \omega_{\text{cg}} \times [\omega_{\text{cg}} \times r_{i/cg}] + \alpha_{\text{cg}} \times r_{i/cg} \quad (8)$$

The arm moment summation in Eq.5 is in equilibrium with,

$\sum M_{x\_arm\_i} = -M_{sxi} + l_{arm} \times \cos(\theta_{arm\_i}) \cdot F_{tyi}$
$\sum M_{y\_arm\_i} = -T_{S\&D\_i} - l_{arm} \times \sin(\theta_{arm\_i})\left(m_w + \frac{m_{arm}}{2}\right) g - l_{arm} \times \cos(\theta_{arm\_i}) F_{txi} + l_{arm} \times \sin(\theta_{arm\_i}) F_{tzi}$
$\sum M_{z\_arm\_i} = -M_{szi} - l_{arm} \times \sin(\theta_{arm\_i})\, F_{tyi} - \text{T}_{\text{self\_i}}$ ……………………. (9)

where $T_{S\&D\_i}$ is the sum of spring and damping torques of the i^{th} arm suspension (spring and damper) as,

$$T_{S\&D\_i}(\theta_{arm\_i}, \dot{\theta}_{arm\_i}) = k_s \times \theta_{arm\_i} + c_d \times \dot{\theta}_{arm\_i} \quad (10)$$

Substituting (6) - (8) into (5), the equation of the arm motion can be obtained as,

$$\left\{I_{arm\_y} + \left(m_w + \frac{m_{arm}}{4}\right) l_{arm}^2\right\} \ddot{\theta}_{arm\_i} = \sum M_{y\_arm\_i} - \left\{I_{arm\_y} + \left(m_w + \frac{m_{arm}}{4}\right) l_{arm}^2\right\} \ddot{\theta} - (I_{arm\_x} - I_{arm\_z})\dot{\phi}\dot{\varphi} + \left(m_w + \frac{m_{arm}}{2}\right) l_{arm}\{\cos(\theta_{arm\_i})\,\ddot{x}_i - \sin(\theta_{arm\_i})\,\ddot{z}_i\} - \left(m_w + \frac{m_{arm}}{4}\right) l_{arm}^2[\sin(\theta_{arm\_i})\cos(\theta_{arm\_i})\,(\dot{\phi}^2 - \dot{\varphi}^2) + \{\cos^2(\theta_{arm\_i}) - \sin^2(\theta_{arm\_i})\}\dot{\phi}\dot{\varphi}] \quad (11)$$

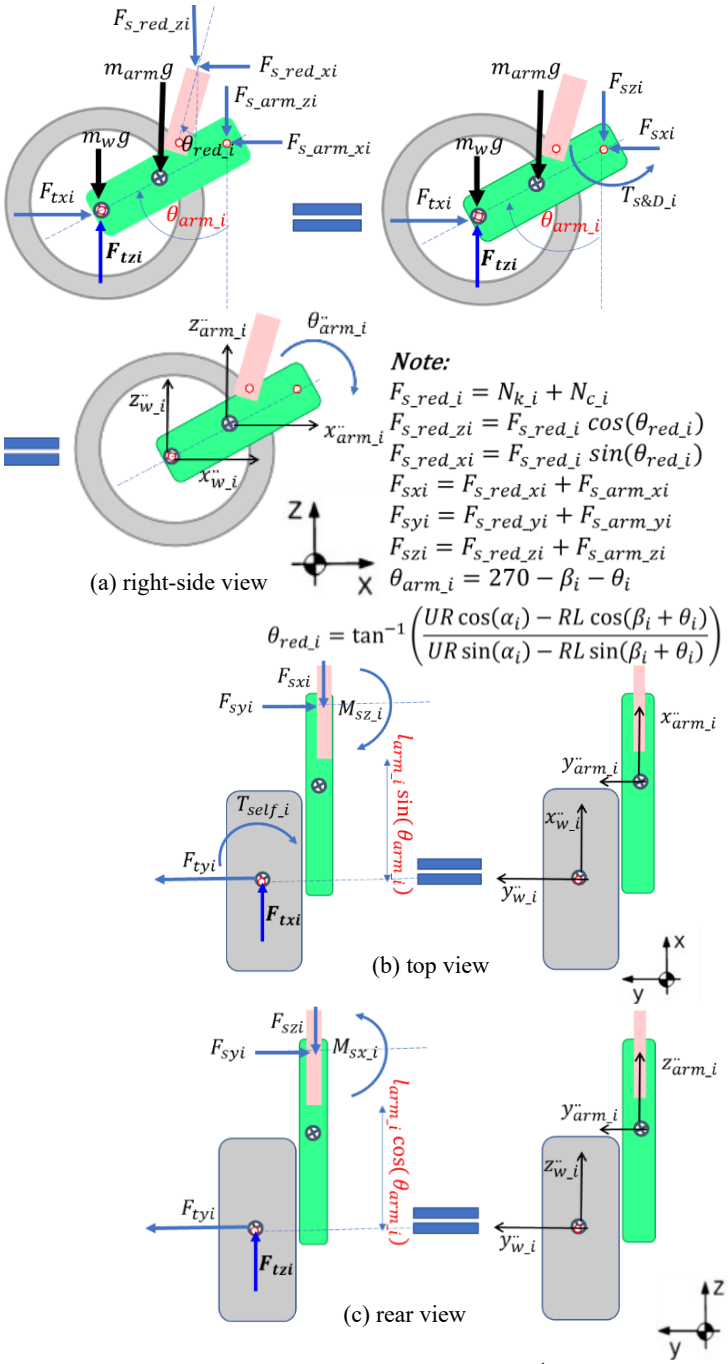

Fig. 5: Dynamic equilibrium of the i^{th} arm and wheel

2.3 Sprung mass dynamic model

The dynamic behavior of the sprung mass is determined in the vehicle model using the internal forces and moments, Fig.6, obtained from the arm dynamic

model. The dynamic equations of the sprung mass can be obtained from the d'Alembert principle [15] as follows:

$$\sum_{i=1}^{6} F_{sxi} = m_s[\dot{v}_x + (v_z\dot{\theta} - v_y\dot{\varphi})]$$
$$\sum_{i=1}^{6} F_{syi} = m_s[\dot{v}_y + (v_x\dot{\varphi} - v_z\dot{\phi})]$$
$$\sum_{i=1}^{6} F_{szi} = m_s[\dot{v}_z + (v_y\dot{\phi} - v_x\dot{\theta})] \quad \ldots\ldots (12)$$

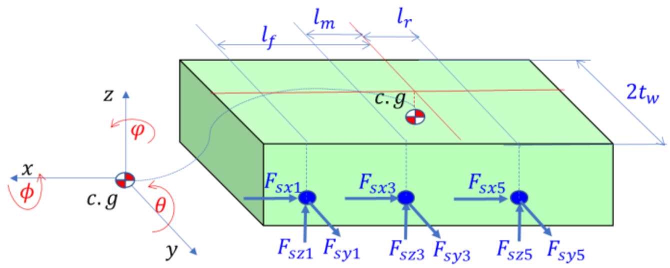

Fig. 6: Vehicle Body (sprung mass) forces

$$\sum_{i=1}^{6} M_{sxi} + t_w\{\sum_{i=1}^{3} F_{sz(2i-1)} - \sum_{i=1}^{3} F_{tz(2i)}\} = I_x\ddot{\phi} + (I_z - I_y)\dot{\theta}\dot{\varphi}$$
$$\sum_{i=1}^{6} T_{S\&D\_i} + \{-l_f \sum_{i=1}^{2} F_{szi} - l_m \sum_{i=3}^{4} F_{szi} + l_r \sum_{i=5}^{6} F_{szi}\} = I_y\ddot{\theta} + (I_x - I_z)\dot{\varphi}\dot{\phi}$$
$$\sum_{i=1}^{6} M_{szi} + t_w\{\sum_{i=1}^{3} F_{sx(2i)} - \sum_{i=1}^{3} F_{sx(2i-1)}\} + \{l_f \sum_{i=1}^{2} F_{syi} + l_m \sum_{i=3}^{4} F_{syi} - l_r \sum_{i=5}^{6} F_{syi}\} = I_z\ddot{\varphi} + (I_y - I_x)\dot{\phi}\dot{\theta} \quad \ldots\ldots (13)$$

3. ESTIMATION ALGORITHM

In order to estimate the tire forces, Kalman filter and manipulated dynamic equation are used. First using Taylor formula and Kalman filter the wheel angular acceleration is estimated based on the measurement of wheel angular speed. Then the corresponding dynamic equations are used to estimate the longitudinal, vertical, and lateral tire forces as shown in Fig.7.

3.1 Longitudinal tire force estimation

To estimate the wheel angular acceleration applying Kalman filter, as system model is derived by Taylor expansion,

$$\omega_i(t+h) = \omega_i(t) + h\dot{\omega}_i(t) + \frac{h^2}{2}\ddot{\omega}_i(t) + d_1$$
$$\dot{\omega}_i(t+h) = \dot{\omega}_i(t) + h\ddot{\omega}_i(t) + d_2$$
$$\ddot{\omega}_i(t+h) = \ddot{\omega}_i(t) + d_3 \quad \ldots\ldots (14)$$
$$\hat{x}(k) = A_{est}\hat{x}(k-1) + L(k)\{y(k) - CA_{est}\hat{x}(k-1)\} \quad \ldots\ldots (15)$$

where h, y, and d are the sampling period, the wheel angular speed measurement and disturbance respectively.

$$A_{est} = \begin{bmatrix} 1 & h & h^2/2 \\ 0 & 1 & h \\ 0 & 0 & 1 \end{bmatrix}, \text{C} = [1 \quad 0 \quad 0]$$

By using (1), the longitudinal tire force can be estimated,

$$\hat{F}_{txi}(k) = \frac{1}{R_i}[T_i(k-1) - J_w \times \hat{\dot{\omega}}_i(k)] \quad \ldots\ldots (16)$$

3.2 Vertical tire force estimation

Based on the steady-state arm dynamics shown in Fig.8, the vertical tire force can be estimated approximately by,

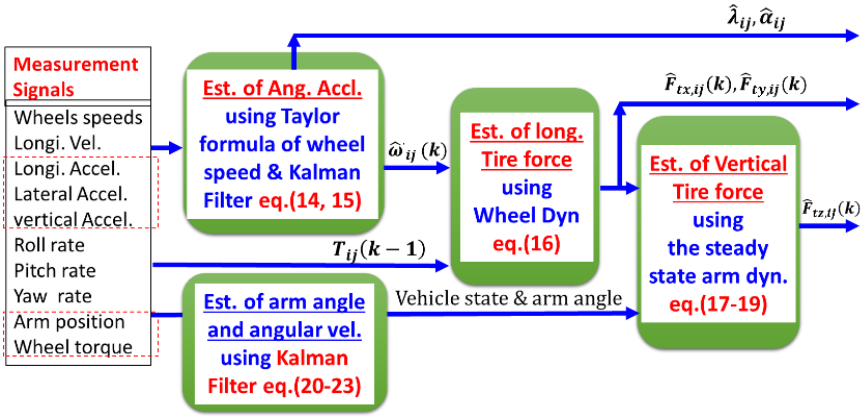

Fig. 7: Scheme for tire forces estimation

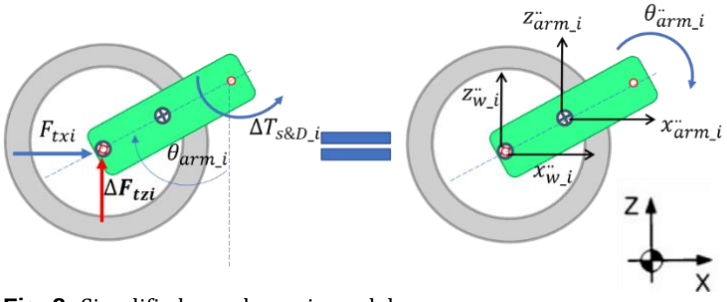

Fig. 8: Simplified arm dynamic model

$$\hat{F}_{tzi}(k) = F_{tzi\_static} + \sum_{i=0}^{N} \frac{\Delta\hat{F}_{tzi}(k-i\Delta t)}{N} \quad \text{..... (17)}$$

$$\Delta\hat{F}_{tzi} = \frac{k_s\Delta\theta_{arm_i} + c_d\Delta\dot{\theta}_{arm_i}}{l_{arm}\sin(\theta_{arm_i})} + \frac{\hat{F}_{txi}}{\tan(\theta_{arm_i})} - \frac{\left(m_w + \frac{m_{arm}}{2}\right)}{\tan(\theta_{arm_i})}\left[a_x \pm t_w\dot{\varphi}\dot{\theta} - l_i(\dot{\theta}^2 + \dot{\phi}^2)\right] + \left(m_w + \frac{m_{arm}}{2}\right)\left[a_z \pm t_w\dot{\phi}\dot{\theta} + l_i\dot{\phi}\dot{\varphi}\right] + l_{arm}\left(m_w + \frac{m_{arm}}{4}\right)\cos(\theta_{arm_i})(\dot{\varphi}^2 - \dot{\phi}^2) + l_{arm}\left(m_w + \frac{m_{arm}}{4}\right)\frac{1-2\sin^2(\theta_{arm_i})}{\sin(\theta_{arm_i})}\dot{\phi}\dot{\varphi} \quad \text{..... (18)}$$

The vertical tire force can be estimated by solving (5) and (9):

$$\hat{F}_{tzi}(k) = \frac{\left[\sum M_{y_{arm_i}}\right] + T_{S\&D\_i} + l_{arm}\times\sin(\theta_{arm\_i})\left(m_w + \frac{m_{arm}}{2}\right)g}{l_{arm}\times\sin(\theta_{arm\_i})} + \frac{\hat{F}_{txi}}{\tan(\theta_{arm\_i})} \quad \text{..... (19)}$$

3.3 Lateral tire force estimation

In case of the low slip condition where, the lateral acceleration of the vehicle is less than 3 m/s^2, the lateral force can be:

$F_{tyi} = -C_\alpha\alpha_i$ ....(20)

, where C_α is the cornering stiffness. Based on the arm dynamic equation (4), the lateral force acting on the sprung mass is,

$F_{syi} = -C_\alpha\alpha_i - (m_{arm} \times \ddot{y}_{arm,i}) + (m_w \times \ddot{y}_{w\_i})$ ..... (21)

By substitute (21) in (12), we have,

$$\sum_{i=1}^{6}[-C_\alpha \alpha_i - (m_{arm} \times \ddot{y}_{arm,i}) + (m_w \times \ddot{y}_{w_i})]$$

$$= m_s[\dot{v}_y + (v_x\dot{\varphi} - v_z\dot{\phi})] \quad \ldots\ldots\ldots\ldots\ldots\ldots\ldots\ldots \ldots\ldots\ldots\ldots\ldots\ldots\ldots\ldots\ldots (22)$$

by solving for the exact value of C_α,

$$C_\alpha = \frac{\{-m_s[\dot{v}_y + (v_x\dot{\varphi} - v_z\dot{\phi})] + \sum_{i=1}^{6}[-(m_{arm} \times \ddot{y}_{arm,i}) + (m_w \times \ddot{y}_{w_i})]\}}{\sum_{i=1}^{6}\alpha_i} \quad \ldots\ldots\ldots\ldots\ldots\ldots (23)$$

Hence, the lateral tire forces $\boldsymbol{F_{tyi}}$ can by calculated from (20).

4. SIMULATION RESULTS AND DISCUSSION

In this section we want to test the estimation algorithm (Eq's 14 to 23). To do that, we used the Eq's (1) – (13) to build Simulink test environment to test the estimation algorithm (using Eq's 14 to 23). Each equation is built as a Matlab function in Simulink. The robotic vehicle parameters are listed in Table 1.

We implemented nine test scenarios to verify the estimation algorithm. In test scenario 1, different input torque to the wheels and same tire longitudinal tire forces are assumed.

T_i= [1; 2; 3; 4; 5; 6] N/m.

F_{txi}= [1; 1; 1; 1; 1; 1] N.

Table1: Parameters of the system dynamic model

Symbol	value	Symbol	value	Symbol	value
$\boldsymbol{m_s}$	833.4kg	m_{arm}	61.2 kg	m_w	44.83 kg
$\boldsymbol{I_x}$	289.8	I_{arm_x}	0.702	I_{w_x}	1.14
$\boldsymbol{I_y}$	915.0	I_{arm_y}	1.5	J_w	1.8
$\boldsymbol{I_z}$	915.0	I_{arm_z}	1.5	I_{w_z}	1.14
$\boldsymbol{l_f}$	0.821 m	l_{arm}	0.351 m	R	0.310 m
$\boldsymbol{l_m}$	0.423 m	$\theta_{arm_F}(0)$	pi/4	k_s	8021 N.m/rad
$\boldsymbol{l_r}$	-0.497m	$\theta_{arm_M}(0)$	3pi/4	c_d	286 N.m.s/rad
$\boldsymbol{t_w}$	0.660 m	$\theta_{arm_R}(0)$	3pi/4		

The resulting wheels angular accelerations are constants. These constants are dependent on T_i (the higher the torque the higher the acceleration). The wheel angular speeds are linear and the wheel angles of rotation are 2^{nd} order as shown in Fig.9.

Based on test scenario 1, the estimated longitudinal tire force starts with a big error since the initial condition can take any unknow value and after 2 sec it converge to the correct estimation as shown in Fig.10.

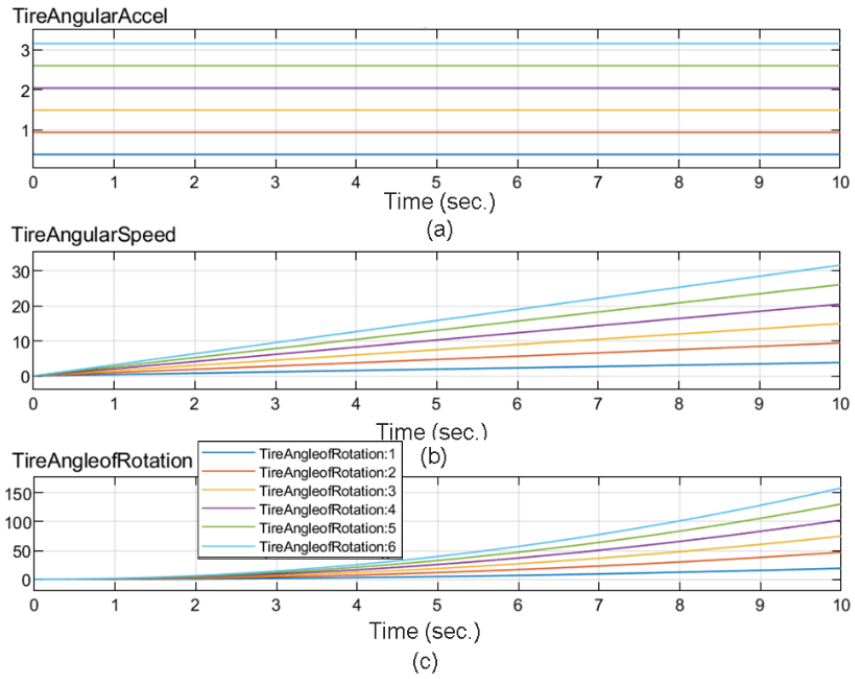

Fig. 9: Test Scenario 1 results on wheel angular acceleration (rad/s^2), angular velocity (rad/s), angle of rotation acceleration (rad).

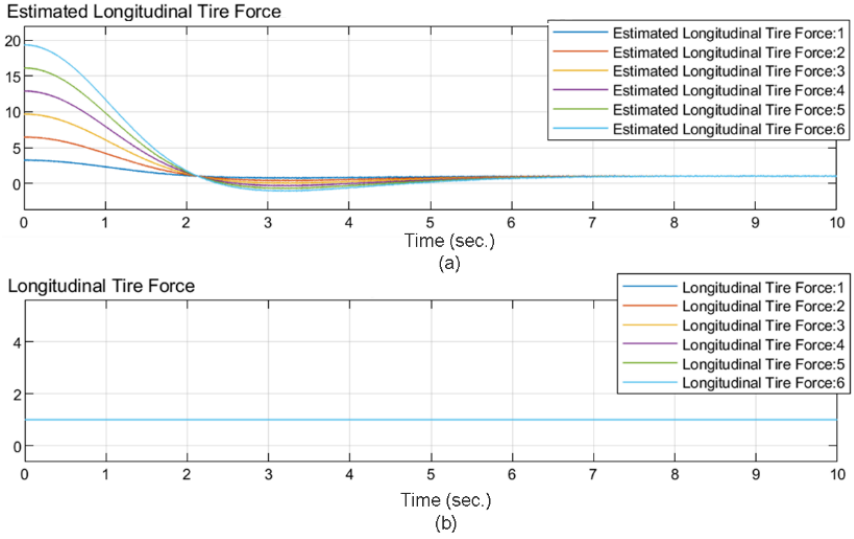

Fig. 10: Estimation of the longitudinal tire force (N)

In Test Scenario 2, we investigate the effect of a sudden change in the longitudinal tire force acting on the first wheel for 2 seconds (at t = 6 to 8 sec). We compared between the results at different estimation matrices sizes.

When estimating the longitudinal tire force with A_{est} of size 3, it takes 1 sec rise time as shown in Fig.11.

We tested several sizes of the system matrix A_{est} as follows;

$$A_{est3} = \begin{bmatrix} 1 & h & h^2/2 \\ 0 & 1 & h \\ 0 & 0 & 1 \end{bmatrix}, \qquad A_{est4} = \begin{bmatrix} 1 & h & h^2/2 & h^3/3! \\ 0 & 1 & h & h^2/2 \\ 0 & 0 & 1 & h \\ 0 & 0 & 0 & 1 \end{bmatrix}$$

$$A_{est5} = \begin{bmatrix} 1 & h & h^2/2 & h^3/3! & h^4/4! \\ 0 & 1 & h & h^2/2 & h^3/3! \\ 0 & 0 & 1 & h & h^2/2 \\ 0 & 0 & 0 & 1 & h \\ 0 & 0 & 0 & 0 & 1 \end{bmatrix}, \quad A_{est10} = \begin{bmatrix} 1 & h & h^2/2 & \cdots & h^9/9! \\ 0 & 1 & h & \cdots & h^8/8! \\ \ldots & 0 & 1 & \cdots & h^7/7! \\ \ldots & \ldots & \ldots & \cdots & \ldots \\ 0 & 0 & 0 & \cdots & 1 \end{bmatrix}$$

Our simulation results in Fig.11, indicate that the rise time is enhanced by increasing the matrix size:

Test Scenario 2: At matrix size 3, the rise time is 1 sec.

Test Scenario 3: At matrix size 4, the rise time is 0.7 sec.

Test Scenario4: At matrix size 5, the rise time: 0.4 sec. (accepted)

Test Scenario 5: At matrix size 10, the rise time is 0.25 sec, but the overshoot (> 40%)

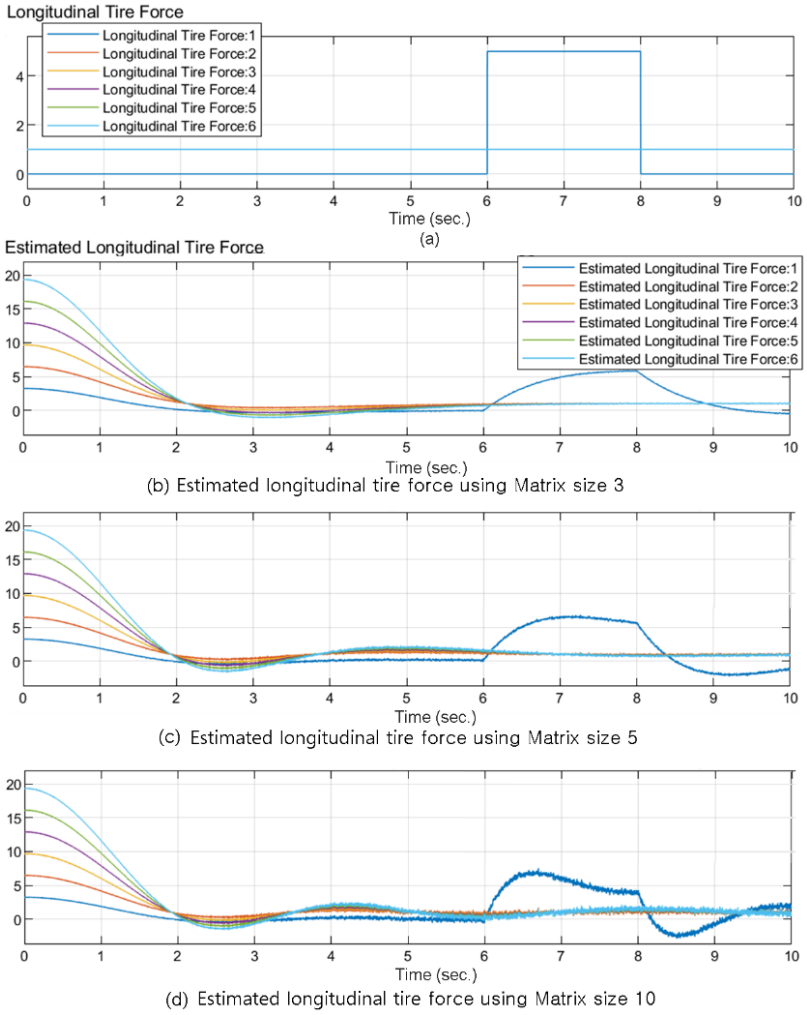

Fig. 11: Estimation of the longitudinal tire force (N) using system matrix sizes of 3, 4, 5, and 10

5. EXPERIMENTAL RESULTS

In order to verify the state estimation algorithm presented in section3 and simulated in section4, we need to access the robotic vehicle with six in-wheel drives but this was not available. We had to scale down the vehicle understudy and fabricate similar small prototype robotic vehicle with six in-wheel drives as show in Fig12.

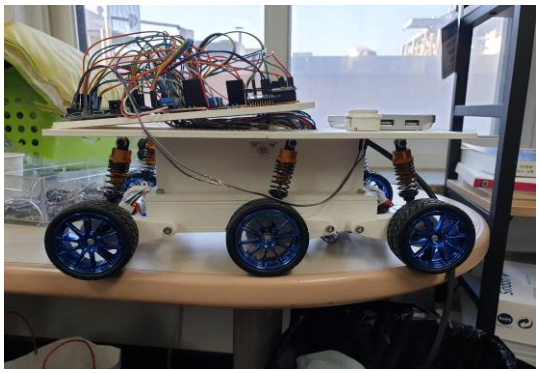

Fig. 12: Small prototype of the robotic vehicle with six in-wheel drives

5.1 States Estimation:

The first experiment is to move forward with constant velocity and stop for two seconds and then return backward in same constant velocity. We used encoder for angle measurements as an input to the estimation algorithm. As shown in Fig.13, the solid red line is the estimation with applying the moving average of size (40 for velocity and 50 for acceleration), the solid blue line is based on Kalman estimator (Matrix size 4), and the green solid line is the raw data.

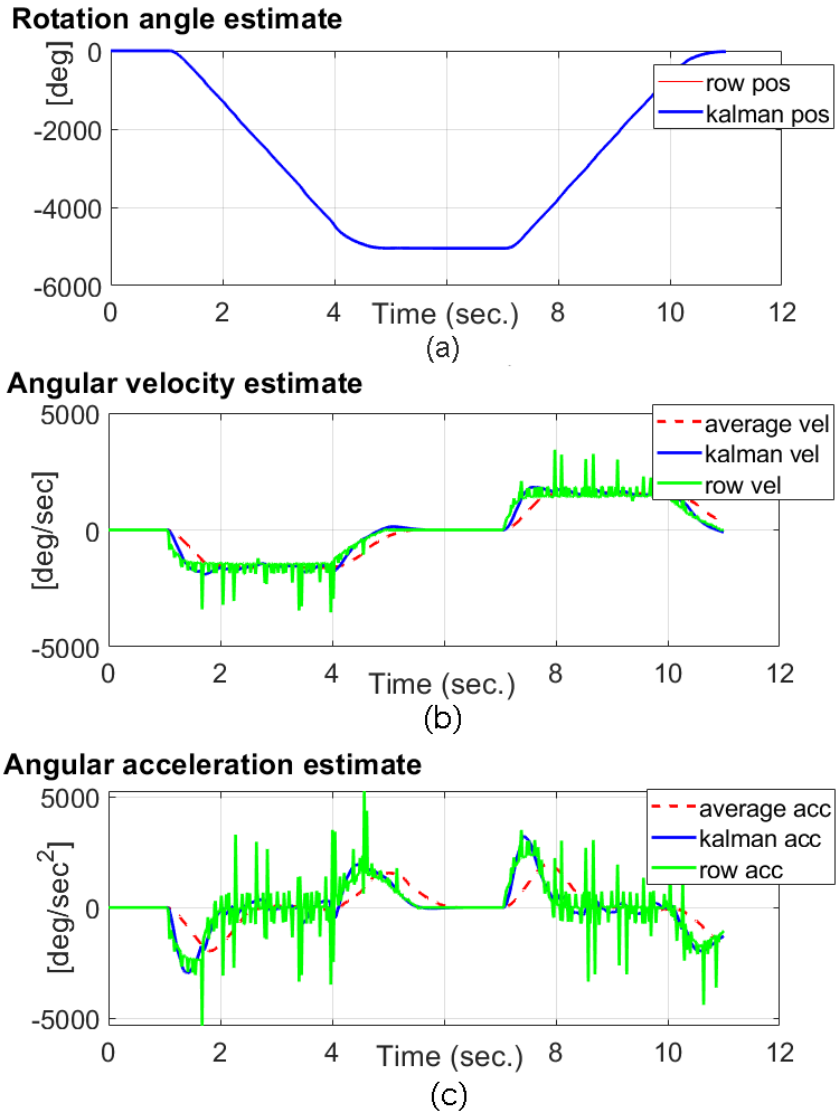

Fig. 13: Angular position, velocity and acceleration estimation

As a result, both the final estimator and the moving average filter removed noise from the raw data. However, the Kalman estimator rather than the moving average filter obtained faster estimation speed and similar estimation results.

5.2 Slip rate estimation:

The second experiment is to estimate the slip ratio on the pavement as shown in Fig.14 and Fig.15. In Fig.14, the black line represents the vehicle speed (IMU measurement), while the blue line-Wheel speed (Apply Kalman filter after measuring Hall sensor).

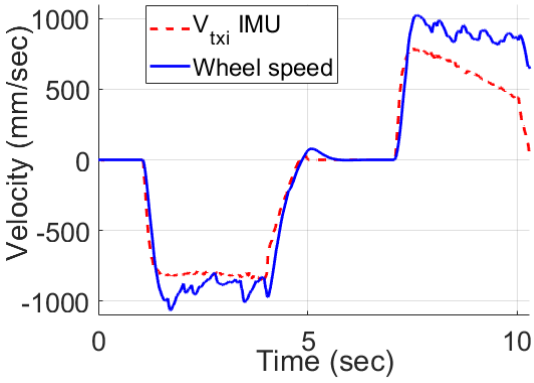

Fig. 14: The 2nd experiment on the pavement, comparing speed of the center of gravity and the wheel speed (R*w)

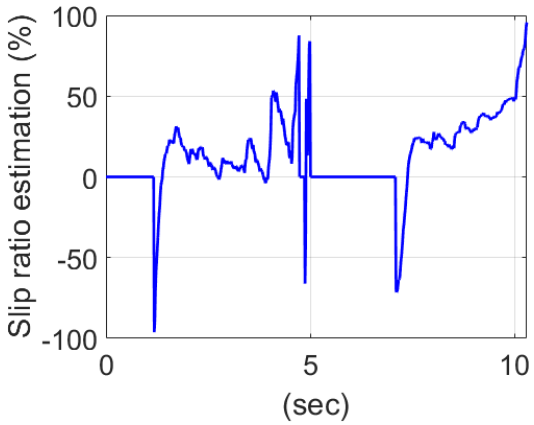

Fig. 15: The 2nd experiment on the pavement, Slip ratio estimation

The average slip rate calculated through 20 experiments under the same conditions was 8.96%. The actual moving distance and the average moving distance measured with the Hall sensor (including slip) were 2590mm and 2817.51mm, respectively, and the ratio to the slip amount was also confirmed to be similar to the slip rate estimated at 8.075%. This indicates that the estimated slip ratio is reliable.

The third experiment is to estimate the slip ratio on off-road driving experiment as shown in Fig.16, Fig.17 and Fig.18. In Fig.17, the red line- is the vehicle speed (IMU measurement), while the blue line-Wheel speed (Apply Kalman filter after measuring Hall sensor)

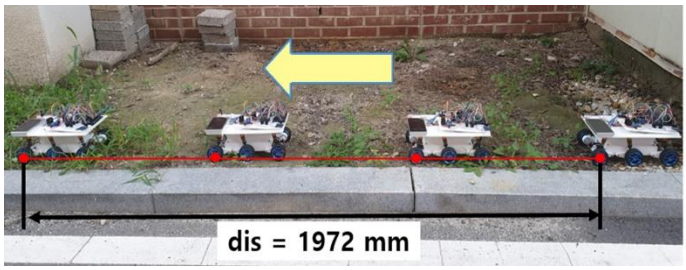

Fig. 16: The 3rd experiment Off-road driving experiment

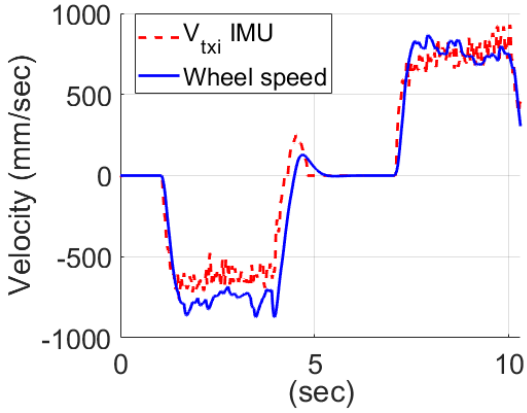

Fig. 17: The 3rd experiment Off-road driving experiment, comparing speed of the center of gravity and the wheel speed (R*w)

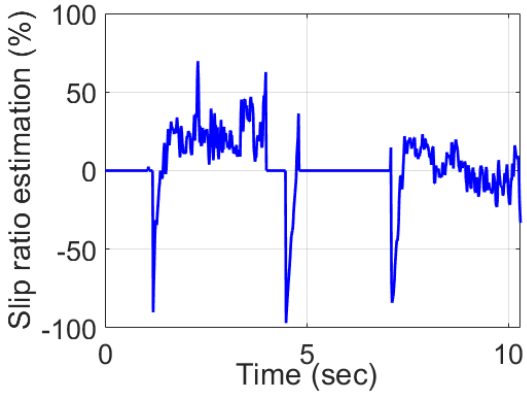

Fig. 18: The 3rd experiment Off-road driving experiment, Slip ratio estimation

The average of the actual moving distance calculated through 20 experiments and the moving distance measured (including slip) by the Hall sensor are 1972mm and 2297.2 mm, respectively. The slip ratio is calculated as 14.19%. As a result of the slip rate estimation, although it has more noise than the flat terrain, the average slip rate is 17.28%. The above experiment also shows data similar to the ratio of slip rate and slip amount. In other words, it was confirmed that the slip rate estimation using the Kalman filter has a high correlation even in irregular terrain.

5.3 Longitudinal tire force estimation:

The fourth experiment is to estimate the longitudinal tire force based on motor current measurement. Based on the motor (Encoder Gear motor: CHR-GM25-370, DC12.0V 350 RPM/1:34) data sheet and the experimental motor torque measurement setup shown in fig.19, the motor constants are estimated as shown in fig.20.

The rated current is 1.7 A, the stall current is 5.6 A, below is the algorithm of estimating the motor torque constant k_t.

If (0 < i <= 1.7) …. where i is the current

k_t= 0.335

If (1.7 <= i <= 5.6)

$$k_t = f(i) = k_{t\_rated} - \frac{i - i_{rated}}{i_{stall} - i_{rated}}(k_{t_{rated}} - k_{t\_stall})$$

$$k_t = 0.335 - \frac{(i - 1.7)(0.124)}{(3.9)}$$

The motor is controlled in our system with PWM. In this case the average voltage changes and the average current changes. Then the torque will be something between the 6V and 12V tables in the motor data sheet. The motor torque Eq.24 can be modified to be Eq.25.

Torque: $T = k_t\, i(t)$ ……(24)

Torque: $T = k_t\, i(t) * (pwm\%)$ ……(25)

Where $pwm\% = \frac{pwm}{255}$

tire weight: 32 gm, Tire weight + motor weight: 144 gm

Tire diameter: 64 mm

Then the moment of inertia can be expressed as:

J_w = 0.5mr^2 = 1.638E-5 Kgm^2

The longitudinal tire force estimation in Eq.16 can be updated in to Eq.26 for the given motor.

$$\hat{F}_{txi}(k) = \frac{1}{0.032}[T_i(k-1) - (1.638\text{E}{-5}) \times \hat{\omega}_i^{\cdot}(k)] \quad ..(26)$$

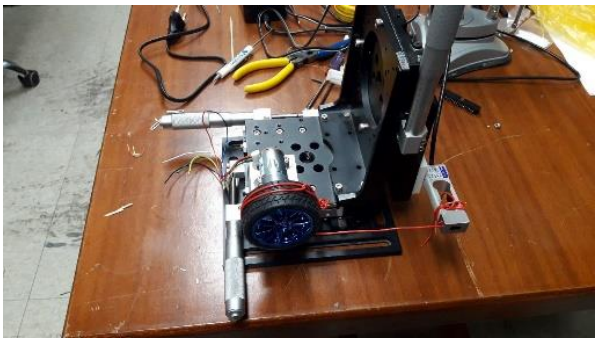

Fig. 19: Experimental setup for motor constants estimation

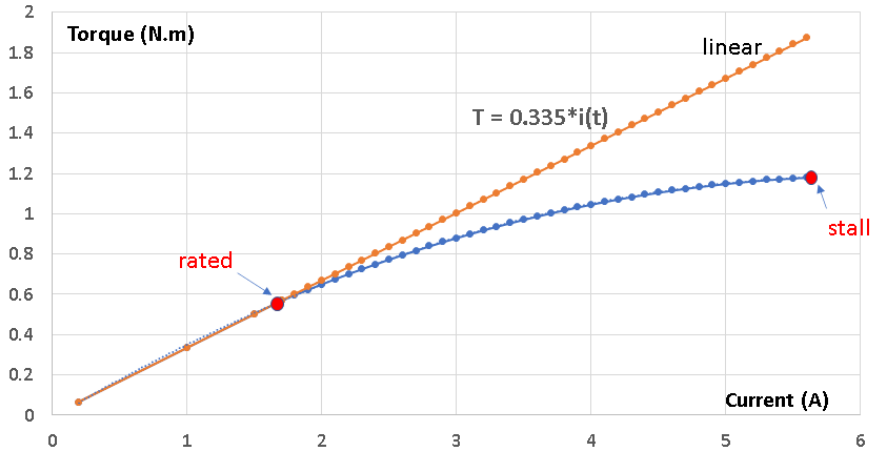

Fig. 20: Non-linear torque constant estimation

6. CONCLUSION

In this research we investigate velocity, acceleration, slip ratio estimation and longitudinal tire force estimation for a six-wheeled robot with articulated suspension. Our estimation algorithm is verified in simulation and experimental tests. Using Kalman filter the wheel angular acceleration is estimated which is used to estimate the longitudinal tire force distribution. Different state estimation matrix sizes are tested. The accepted response in for matrix size 5 with rise time 0.4 sec and overshoot < 20%.

Then a small prototype of the robotic vehicle with six in-wheel drives is fabricated for experimental verification of the estimation algorithm. Four experiments are executed in pavement and off-road driving to estimate the wheel angular position, velocity and acceleration states and finally the slip ratio is estimated in these situations. We found experimentally that the slip rate estimation using the Kalman filter has a high correlation even in irregular terrain. Moreover, the longitudinal tire force estimation law for the given motor is then formulated.

ACKNOWLEDGEMENTS

This research was supported by a grant from Defense Acquisition Program Administration and Agency for Defense Development under contract UD180045RD.

REFERENCES

[1] X. Zhu, Y. Kim, Mark A. Minor, C. Qiu, "Autonomous Mobile Robots in Unknown Outdoor Environments", CRC Press, (2017).

[2] Moustapha Doumiati, Ali Charara, Alessandro Victorino, Daniel Lechner, Bernard Dubuisson, "Vehicle Dynamics Estimation using Kalman Filtering", John Wiley & Sons, Inc., (2013).

[3] Blundell, M.; Harty, D. The Multibody Systems Approach to Vehicle Dynamics; ElSevier, (2004).

[4] Manuel Acosta, Stratis Kanarachos, and Mike Blundell, “Review: Road Friction Virtual Sensing: A Review of Estimation Techniques with Emphasis on Low Excitation Approaches”, Applied Sc. (2017).

[5] Hrgetic, M.; Deur, J.; Ivanovic, V.; Tseng, E., "Vehicle sideslip angle EKF Estimator based on Nonlinear Vehicle Dynamics Model and Stochastic Tire Forces Modeling", SAE Int. J. Passeng. Cars Mech. Syst., 7, 86–95, (2014).

[6] Mantaras, D.; Luque, P.; Nava, J.; Riva, P.; Giron, P.; Compadre, D.; Ferran, J. "Tyre-road grip coefficient assessment. Part 1: Off-line methodology using multibody dynamic simulation and genetic algorithms", Veh. Syst. Dyn. Int. J. Veh. Mech. Mob., 51, 1603–1618, (2013).
[7] Ghandour, R.; Victorino, A.; Doumiati, M.; Charara, A. "Tire/Road Friction Coefficient Estimation Applied to Road Safety. In Proceedings of the Mediterranean Conference on Control and Automation, MED, Marrakech, Morocco,(2010).
[8] E. Nada, A. Ahmed, M. Abd-Alla, "Modified dual unscented kalman filter approach for measuring vehicle states and vehicle parameters", Int. J. Eng. Res. Technol., vol. 3, (2014).
[9] Nah, J., Seo, J., Yi, K., Kim, W., & Lee, J. , " Friction circle estimation-based torque distribution control of six-wheeled independent driving vehicles for terrain-driving performance" Proceedings of the Institution of Mechanical Engineers, Part D: J. of Automobile. Eng., 229(11), (2015).
[10] H. Hamann, J. K. Hedrick, S. Rhode and F. Gauterin, "Tire force estimation for a passenger vehicle with the Unscented Kalman Filter," 2014 IEEE Intelligent Vehicles Symposium Proceedings, Dearborn, MI, pp. 814-819, (2014).
[11] A. Rezaeian et al., "Novel Tire Force Estimation Strategy for Real-Time Implementation on Vehicle Applications," in IEEE Transactions on Vehicular Technology, vol. 64, (2015).
[12] A. Zareian, S. Azadi, and R. Kazemi, “Estimation of road friction coefficient using extended Kalman filter, recursive least square, and neural network”, J. of M.b. Dyn., (2015).
[13] Y. Kim, “Motion State Estimation for an Autonomous Vehicle-Trailer System using Kalman filter-based Multisensor Data fusion”, Int.l J.: Asia Life Sciences Supplement 11: 81-92, (2015).
[14] Hussein F. M. Ali, Nader A. Mansour, Y. Kim, "Comparative Study of Extended and Unscented Kalman Filters for Estimating Motion States of An Autonomous Vehicle-Trailer System", Int. Conf. Recent Dev. in Mechanical Eng., (ICRAME), (2020).
[15] J. Kang, W. Kim, J. Lee, and K. Yi, “Skid steering-based control of a robotic vehicle with six in-wheel drives”, Proc. IMechE Vol. 224 Part D: J. Automobile Engineering, (2010).
[16] Hussein F. M. Ali, Se-Woong Oh, Youngshik Kim, "State Estimation Of A Robotic Vehicle With Six In-Wheel Drives Using Kalman Filter", ASME Int. Conf. Information Storage and Processing Systems, ISPS2020, June 25-26, 2020, Milpitas, CA, USA. (2020).
[17] “Adams Manual: Tire Models, Using the Fiala Handling Force Model”, MSC Software Corporation.
https://www.mscsoftware.com/ [Accessed 2-3-2020].